Remote Sensing of Environment 144 (2014) 172–178

Contents lists available at ScienceDirect

Remote Sensing of Environment

journal homepage: www.elsevier.com/locate/rse

The effect of particulate organic content on the remote sensing of marine suspended sediments

D.G. Bowers [a,*], P.S. Hill [b], K.M. Braithwaite [a]

[a] School of Ocean Sciences, Bangor University, Menai Bridge, Anglesey LL595AB, UK
[b] Department of Oceanography, Dalhousie University, Halifax, Nova Scotia B3H 4R2, Canada

ARTICLE INFO

Article history:
Received 9 September 2013
Received in revised form 6 December 2013
Accepted 6 January 2014
Available online 11 February 2014

Keywords:
Backscattering efficiency
Particle mineral content

ABSTRACT

We report on the relationship between the backscattering coefficient at 665 nm and the cross sectional area of particles in suspension in the Irish Sea, Celtic Sea and English Channel. A plot of the backscattering coefficient against particle area shows two distinct trends: one for particles with high mineral content and another for particles with low mineral content. Backscattering per unit particle area (effective backscattering efficiency, Q_{bb}) shows a continuous non-linear dependence on the ratio of mineral to total suspended solids (*MSS/TSS*) over the range $0.35 < MSS/TSS < 0.91$. The relationship can be represented by an exponential function: $Q_{bb} = 0.000087 \exp(6.9\ MSS/TSS)$, which explains 62% of the observed variance in backscattering efficiency. Changes in particle size have no significant influence on Q_{bb}. As the *MSS/TSS* ratio increases, the backscattering ratio (b_b/b) also increases. The implication for the quantitative remote sensing of marine suspended sediments is that the mass specific backscattering coefficient, b_b^* depends on the particle area per unit mass multiplied by a function which depends on the mineral content of the particles.

1. Introduction

The remote sensing of the ocean in the visible part of the spectrum relies on the fact that some of the sunlight entering the sea is backscattered by the water itself and by large numbers of mainly microscopic particles suspended near the surface. In the open ocean, these particles are mostly organic: phytoplankton cells and their detrital products. As the coast is approached, organic particles are supplemented by inorganic particulate material introduced by rivers and lifted off the sea bed. In shelf seas and estuaries, a mixture of organic and inorganic particles, present in large numbers and possessing a high refractive index, can become the main source of backscattered light (Stramski, Boss, Bogucki, & Voss, 2004). This fact has proved useful in the remote sensing of suspended sediments in shallow waters. Satellite data has been used to map the distribution and temporal changes of particle loading (Binding, Bowers, & Mitchelson-Jacob, 2005; Doxaran, Froidefond, Castaing, & Babin, 2009; Neil, Cunningham, & McKee, 2011; Rivier et al., 2012) and has led directly to a better understanding of the physics of particles in seawater (Bowers, Boudjelas, & Harker, 1998; Ellis, Binding, Bowers, Jones, & Simpson, 2008; Gallegos, Werdell, & McClain, 2011; Neil, Cuningham, McKee, & Polton, 2012).

There have been a number of papers on the backscattering of light by the mainly organic particles in the ocean (Ahn, Bricaud, & Morel, 1992; Boss et al., 2004; Vaillancourt et al., 2004; Westberry, Dall'Olmo, Boss, Behrenfeld, & Moutin, 2010), and in recent years there have been advances in our understanding of the structure and optical properties of the type of particle found in coastal waters. When particles are present in high concentrations, the water is turbulent, and there is a mixture of organic and mineral material, the particles flocculate into aggregates of complex shape (Eisma et al., 1990; Gregory, 1989; Khelifa & Hill, 2006). Aggregates are far from spherical, a mixture of individual pieces of solid material of different refractive indices with water in the gaps between the solids. It is the factors that affect the backscattering of light by these aggregates that concern us in this paper.

It is difficult to say how these complex structures will interact with light. Mie theory, which deals with solid spheres, hardly seems appropriate, although some progress has been made in modelling the optical properties of aggregates by considering them to be composed of concentric shells of different refractive indices (Boss, Slade, & Hill, 2009). It is likely that the optical properties of an aggregate depend upon its size, shape, density and refractive index. Some simplification of the problem can be achieved by considering optical properties *per unit area*, since size, shape and density control the cross sectional area per unit mass. Although more difficult to measure in situ than mass concentration, particle area can be measured with underwater cameras, conventional (Eisma et al., 1990; Milligan, 1996) and holographic (Graham & Nimmo-Smith, 2010), and inferred from laser diffraction measurements (Agrawal & Pottsmith, 2000). The ratio of the backscattering coefficient to the cross sectional area of the particles per m^3 of water is the backscattering efficiency; there are equivalent efficiencies for scattering and absorption (all dimensionless). The term *efficiency* in this sense strictly refers to a suspension of uniform particles but in this paper we will expand its use to a natural suspension of particles with a range of sizes

* Corresponding author.
E-mail address: d.g.bowers@bangor.ac.uk (D.G. Bowers).

0034-4257/$ – see front matter © 2014 Elsevier Inc. All rights reserved.
http://dx.doi.org/10.1016/j.rse.2014.01.005

and properties by thinking of it as an effective efficiency for that suspension. For solid, spherical particles the scattering and backscattering efficiency depend on the refractive index of the particles and, for particles of size comparable to the wavelength of light, or smaller, the efficiency will depend on the particle size.

There have been relatively few studies of the way that the backscattering efficiency depends on the particle type. An important result was obtained by Flory, Hill, Milligan, and Grant (2004) working in the Bedford Basin, Nova Scotia. These authors used an in situ camera to measure particle area and a HOBI Labs Hydroscat-6 backscattering sensor to measure the backscattering coefficient. They showed that the effective backscattering efficiency decreased by a factor of 3 after the advent of a phytoplankton bloom, when the proportion of organic particulate material increased. In measurements in western Europe and French Guyana, Neukermans, Loisel, Meriaux, Astoreca, and McKee (2012) found that backscattering efficiency increased by about an order of magnitude from organic-dominated to mineral-dominated particles. The mineral content of the particle was the main driver (rather than size or density) of variations in backscattering per unit area.

Backscattering coefficients can be measured with commercially available instruments (Boss & Pegau, 2001). In this work, we take a different approach to measuring backscattering: calculating it from reflectance and total absorption measurements. This method requires some assumptions, but we think these are reasonable. Backscattering determined from reflectance is a little closer to the remote sensing signal in that it includes photons that are scattered several times at small angles before joining the upwelling photon flux.

Although refractive index of particles is difficult to measure directly, it is expected to depend upon the mineral content (since minerals have a higher refractive index that of typical marine organic material (Babin, Morel, Fournier-Sicre, Fell, & Stramski, 2003)). Our aim in this paper is therefore to examine how the backscattering efficiency depends on the proportion of mineral matter in the total solid matter in suspension, on the chlorophyll content and on particle size. We use measurements in the red part of the spectrum (665 nm) which is most sensitive to variations in concentration of suspended sediments in moderately turbid water (Binding et al., 2005; Neil et al., 2011).

2. Methods

Observations were made at 10 sites, and 97 stations, along the west coast of Great Britain, first in 2002, and then during the period June 2008 to July 2009 (Table 2 and Fig. 1). The sites have varied optical properties ranging from deep clear water in the Clyde Sea in the north and the Celtic Sea in the south to shallow turbid water in the Irish Sea. The observations to the north of Anglesey (site 5) were made during a phytoplankton bloom. Observations were made in the Menai Strait on two occasions, one on a spring tide, the other at neaps and these are treated as two different 'sites' in the analysis that follows. (See Table 2.)

Table 1
Notation.

A	Cross sectional area of suspended particles per unit volume of water, units m^{-1}
A_X,A_C	Cross sectional areas measured by LISST 100X and 100 type C, respectively
a	Total absorption coefficient, units m^{-1}
a_W, a_P, a_D	Partial absorption coefficients of water, particles and dissolved material, m^{-1}
b	Scattering coefficient, m^{-1}
b_b	Backscattering coefficient, m^{-1}
b_b^*	Mass-specific backscattering coefficient $= b_b/TSS$, units $m^2\ g^{-1}$
D_A	Sauter diameter, units μm
E_S,E_D,E_U	Irradiance, downwelling above surface, downwelling below surface and upwelling below surface respectively, units photons $m^2\ s^{-1}$
f	Factor depending on ambient light conditions that links reflection coefficient to absorption and backscattering coefficients. Dimensionless.
MSS	Mass concentration of mineral suspended solids, $mg \cdot l^{-1}$
R	Irradiance reflection coefficient $= E_U/E_D$ measured just below the sea surface
TSS	Mass concentration of total suspended solids, $mg \cdot l^{-1}$
Q_{bb}	Effective backscattering efficiency $= b_b/A$. Dimensionless
λ	Wavelength of light, nm
μ_0	Mean value of the cosine of angle photons make with the vertical, measured just below the sea surface

Table 2
Observation sites and symbols used on figures.

Site	Location	No. of stations	Month	Symbol
1	Inchmarnock Water, Clyde Sea	1	July 2009	Open square
2	Burrow Head	8	July 2009	Closed square
3	Solway Firth	4	July 2009	Open triangle
4	Conwy Bay	12	July 2009	Open circle
5	North Anglesey	5	April 2009	Closed circle
6	Anglesey (west)	12	April 2009	Closed triangle
7	Menai Strait (neap tide)	12	Sept 2008	Plus
8	Menai Strait (spring tide)	7	Sept 2008	Asterisk
9	Plymouth Sound	7	June 2008	Closed diamond
10	Celtic Sea	29	July 2002	Cross

2.1. Radiometer measurements

At each station sub-surface irradiance reflection coefficients $R(\lambda)$ were measured with a Biospherical Instruments PRR600 radiometer. This instrument measures radiance and irradiance in 6 wavebands (Binding et al., 2005). Underwater irradiance measurements were normalised by dividing by above surface irradiance E_S, measured with a separate instrument with six equivalent channels, to correct for variations in cloud cover during the profiling.

Two underwater profiles were made, each down to a depth of 10 m (little light penetrates beneath this depth in these waters). In the first profile, the instrument was oriented to measure downwelling irradiance, E_D; it was then inverted and a second profile of upwelling irradiance E_U was made. Upwelling irradiance and downwelling irradiance (normalised by surface irradiance) were extrapolated to the sea surface by plotting the logarithm of the ratios E_D/E_S and E_U/E_S at each wavelength against depth and fitting a straight line to the data. The irradiance reflection coefficient just below the sea surface was calculated as the intercept of this line at zero depth, that is:

$$R(\lambda) = \frac{E_U(\lambda, 0-)}{E_D(\lambda, 0-)} \tag{1}$$

where the symbol *0–* refers to a value at zero depth but just below the sea surface. (see Table 1 for a list of symbols used in this paper).

The diffuse attenuation coefficient for downwelling irradiance, $K_D(\lambda)$ was calculated by plotting the natural logarithm of E_D against depth and fitting a straight line to the data. The absolute value of the slope of the line is equal to the diffuse attenuation coefficient. We report here the values for the diffuse attenuation coefficient of white light $K_D(\mathrm{PAR})$.

2.2. Calculating backscattering coefficients

The irradiance reflection coefficient just below the surface is related to the bulk backscattering and absorption coefficients of near surface waters by

$$R = f\frac{b_b}{a + b_b} \tag{2}$$

where f is a parameter which depends on the angular distribution of the light entering the sea, b_b is the backscattering coefficient and a is the total absorption coefficient (Gordon, Brown, & Jacobs, 1975; Kirk,

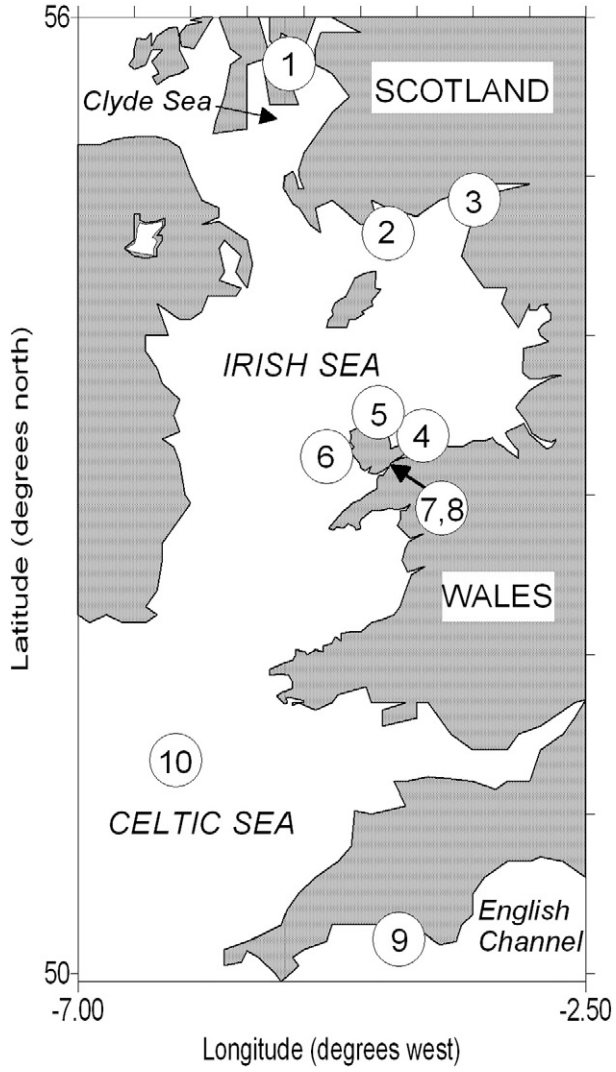

Fig. 1. Map of the study area showing location of sites where samples were collected. Names of sampling sites and number of stations at each are given in Table 2.

2011). The dependence of R, b_b and a on wavelength λ has been omitted from this and subsequent equations for brevity. Rearranging Eq. (2) for the backscattering coefficient gives:

$$b_b = \frac{1}{f - R} Ra. \tag{3}$$

The parameter f was calculated from equations given in Kirk (2011)

$$f = 0.975 - 0.629\mu_0 \tag{4}$$

where μ_0 is the average cosine of the angle photons make with the vertical just below the sea surface. The average cosine was calculated from the solar elevation and a visual estimate of the proportions of diffuse and direct sunlight. The mean value of f for this study was 0.43 with a standard deviation of 0.016.

The total absorption coefficient a was calculated as the sum of absorption by water (W), particles (P) and dissolved material (D):

$$a = a_W + a_P + a_D. \tag{5}$$

The absorption coefficient of sea water was taken from Pope and Fry (1997). Water samples were collected at 1 m below the surface and analysed for particle and dissolved absorption coefficients. Particle absorption was measured by filtering a known volume of sea water through Whatman GF/F filters and then measuring the absorption coefficient of the particles on the filter in a Shimadzu UV-1601 dual beam spectrophotometer, using a clean filter as a reference blank. The absorption coefficient was corrected for the effects of pathlength amplification in the particles and the filter using the method of Cleveland and Weidemann (1993). The absorption coefficient of dissolved material passed through a 0.2 μm filter was measured in a 10 cm cell in the same spectrophotometer, using distilled water as a blank.

Total absorption at 665 nm calculated using Eq. (5) was substituted into Eq. (3) and used with the measurements of reflection to calculate the backscattering coefficient at 665 nm. Note that there is a potential inconsistency in the measurements here: reflection coefficients are the average from zero down to 10 m and the absorption coefficients were measured in the surface metre. However, the reflection coefficients showed very little variability with depth and we do not consider the difference in the scale of the measurements to be a problem.

2.3. Particle cross sectional area, size and scattering coefficients

At each station, a profile was made with a Sequioa LISST in-situ particle sizer. This instrument uses the diffraction pattern of suspended matter that intercepts its laser beam to infer the volume of particles in 32 logarithmically-spaced size classes in the range 2.5 to 500 μm. The cross sectional area of particles in unit volume of water was calculated by summing the area of particles in each size class, assuming they are spheres of diameter equal to the mid-point of the class. The average cross sectional area of the particles in the top 10 m of the profile was calculated, to be consistent with the reflection coefficients.

Two LISST instruments were used in this work, a LISST 100 type C and a LISST 100X, both operating over the size range 2.5–500 μm. On a number of occasions, both instruments were profiled together on separate frames and this allowed a cross-calibration to be made. A linear regression of the particle area measured by the LISST C on these occasions against that measured by the LISST X gave the equation:

$$A_X = 0.0158 + 0.897A_C \tag{6}$$

where A_X is the cross-sectional area measured by the LISST X and A_C that by the LISST C. R^2 for this regression was 0.91. Eq. (5) was applied to the cross-sectional areas measured by the LISST C to converge the measurements from the two instruments.

Concerns have been expressed over the reliability of LISST measurements: there are discrepancies between the cross-sectional area of particles measured by laser diffraction and those measured with holographic cameras (Graham et al., 2012). These discrepancies arise because particles are not spherical and have a range of sizes that extend beyond that measured by the LISST, leading to aliasing. A thoughtful discussion of this issue is given in Fugate and Friedrichs (2003). It is therefore advisable to consider the particle cross sectional areas reported here as relative, rather than absolute, although the numerical values of backscattering efficiency we report in the results section are consistent with results in the literature, obtained with photographic measurements of particle area.

As a measure of particle size we used the Sauter diameter (D_A) equal to 3/2 times the total volume of the particles divided by their total cross-sectional area. Sauter diameter is sometimes favoured in optical studies because, when divided into the volume of particles, it gives a measure of cross sectional area.

The scattering coefficient, b, can be estimated by integrating the light collected by the 'rings' of the LISST instruments. The LISST measures light scattered forward at an angle of less than 9° from the original beam direction. Since most light is scattered by particles at small angles, nearly all of the total scattered light is caught by the LISST. Values of b measured in this way compare well with those measured in other ways (Bowers, Braithwaite, Nimmo-Smith, & Graham, 2011). There is a small difference in wavelength between these and the backscattering

measurements. The LISST laser operates at 670 nm and the backscattering coefficient was calculated at 665 nm.

2.4. Gravimetric measurements of total and mineral suspended matter

The mass concentration of particles was measured by filtering a known volume of surface sea water through pre-weighed, pre-combusted, Whatman GF/F filters. The concentration of total suspended matter (*TSS*) was calculated from the increase in weight of the filter after drying. Filters were then baked in an oven at 500 °C for 3 h to remove organic matter, cooled and re-weighed to give the concentration of mineral suspended matter (*MSS*). Triplicate samples were taken at each station and an average taken. If one of the samples gave significantly different weights to the other two, this was discarded in the averaging.

3. Results

The mean values of parameters measured at each site are summarised in Table 3. The clearest waters sampled were in the Clyde Sea and the most turbid in the Menai Strait. There is a factor of 20 in the value of reflection coefficient between these sites (and a factor of 30 in the backscattering coefficient). The range of particle area and K_D(PAR) is more modest, but still varies by an order of magnitude over the sites; mass concentration varies by just a factor of 3. At most sites, the *MSS/TSS* ratio is typical of that found in shelf seas and estuaries: over 75%, but at two sites (5 and 10) the mineral proportion is less than 70%.

3.1. Relationship between reflection and backscattering coefficients

Fig. 2 shows a plot of the measured irradiance reflection coefficient at 665 nm against the backscattering coefficient calculated with Eq. (3). As noted before (Binding et al., 2005) there is a strong relationship between reflectance and scattering (and, in this case, backscattering) in these waters. For reflectance measurements in the red part of the spectrum for low to moderate values of b_b, the denominator in Eq. (2) shows little variability as absorption by water is the dominant term. At the highest values of backscattering measured in this data set, the gradient of the R:b_b relationship reduces as backscattering and absorption by particles contribute more to the denominator in Eq. (2).

3.2. Backscattering coefficients and particle area

Fig. 3 shows the backscattering coefficient at 665 nm plotted against the LISST-estimate of the cross-sectional area of particles in suspension. The data appears to fall into two groups. In one group there is a general, although somewhat scattered, increase in backscattering as the particle area increases. In the second group, there is no evidence that the backscattering coefficient increases as the particle area increases. This second group of data points is composed of observations from site 10 (the Celtic Sea) and site 5 (north Anglesey). In both these data sets, the mean *MSS/TSS* ratio was less than 0.7.

Table 3
Mean values of parameters measured.

Site	b_b m^{-1}	*TSS* ($mg \cdot l^{-1}$)	*MSS/TSS*	K_D(PAR) m^{-1}	R(665)	D_A (μm)	A (m^2/m^3)
1	.0014	5.09	0.79	0.17	.0014	23.1	0.15
2	.0048	3.91	0.86	0.22	.0043	38.9	0.16
3	.0209	6.47	0.82	0.39	.0164	30.4	0.52
4	.0163	6.82	0.83	0.41	.0126	38.9	0.58
5	.0042	4.12	0.64	0.36	.0031	20.7	0.96
6	.0077	4.47	0.81	0.25	.0069	35.7	0.28
7	.0421	10.28	0.85	1.06	.0280	52.8	1.41
8	.0352	13.96	0.82	0.76	.0230	37.8	1.50
9	.0121	2.39	0.79	0.37	.0104	28.7	0.43
10	.0036	2.39	0.63	0.18	.0033	54.4	0.50
All	.0142	5.55	0.79	0.40	.0106	42.6	0.38

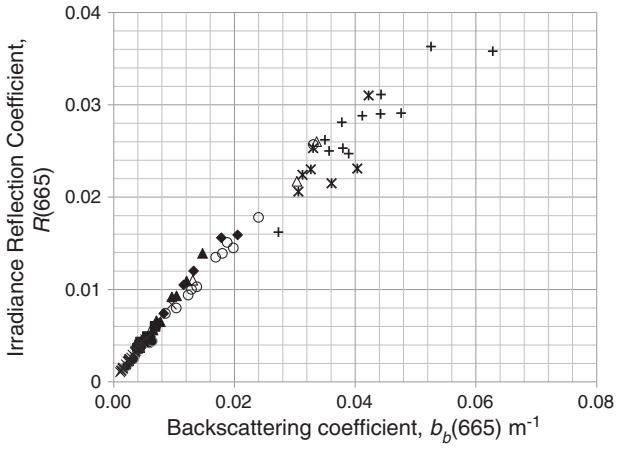

Fig. 2. Irradiance reflection coefficient at 665 nm at each station plotted against the backscattering coefficient at the same wavelength calculated using Eq. (3). A list of the symbols used on this and subsequent plots in this paper are shown in Table 2.

At the high end of the backscattering range, it is noticeable that the Menai Strait neap tide data has a higher value of b_b than at the same site at spring tides, even though the area of particles in suspension was about the same. The neap tide data also had a slightly higher mineral content.

3.3. Backscattering per unit particle area as functions of MSS/TSS and particle size

Fig. 4 shows the backscattering coefficient at 665 nm divided by the particle cross-sectional area (to form the effective backscattering efficiency, Q_{bb}) plotted against the mineral-to-total particle mass ratio (*MSS/TSS*). All ten sites now show a continuous trend in which backscattering efficiency remains constant and low (below 0.01) until the mineral content of the particles reaches about 70%, at which point the efficiency starts to increase up to a maximum of 0.051 for 90% mineral content. Aggregates with high mineral content are much better at backscattering light than ones with low mineral content and the same cross sectional area, presumably because they have a higher refractive index. We can compare these results for backscattering efficiency with those in the literature. Flory et al. (2004) report values of $Q_{bb} = 0.01$ before an algal bloom when particles were mostly inorganic and 0.003 during the bloom. These values are a little lower than those reported here. Neukermans et al. (2012) reports values of $Q_{bb} = 0.04$ in mineral dominated (case 2) water and 0.01 in open ocean (case 1) waters. These values are entirely consistent with our measurements. Stramski et al.

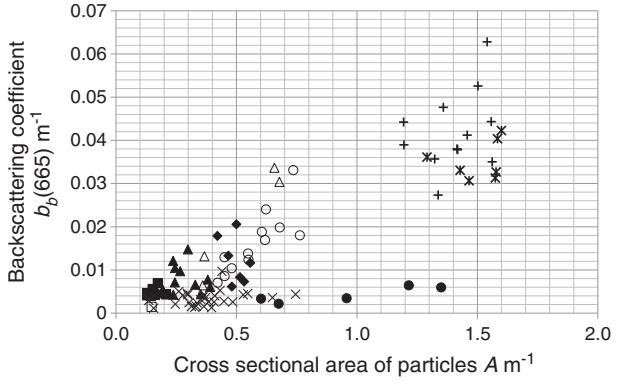

Fig. 3. Backscattering coefficient at 665 nm (from Eq. 3) plotted against the cross sectional area of particles per unit volume of water, measured by the LISST.

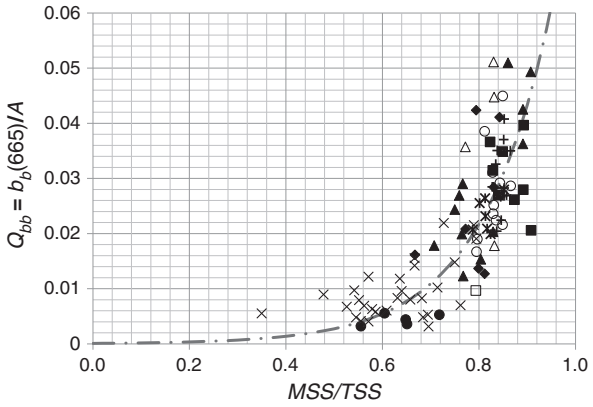

Fig. 4. Backscattering efficiency Q_{bb} at 665 nm plotted against the ratio of mineral to total suspended solids *MSS/TSS*. The dashed line shows the fitted curve represented by Eq. (8).

(2004) examined the effect of particle mineral content on backscattering efficiency on theoretical grounds and estimated that there would be an increase in Q_{bb} by a factor of 30 from purely organic to purely mineral particles, although they stress that the exact value of the range of values depended on some of the assumptions made in their model.

At the present state of our understanding of the interaction of light with particles, there is no exact theory for the backscattering efficiency of real particles in the sea. However, it is useful to fit a functional relationship to the data in Fig. 4 for some of the calculations which we will perform later. By definition, the backscattering coefficient can be written as the product of backscattering efficiency and particle area per unit volume of water:

$$b_b = Q_{bb}A. \tag{7}$$

We sought a functional relationship between Q_{bb} and *MSS/TSS* in the form of an exponential curve, that is

$$b_b = c_1 \exp(c_2.MSS/TSS)A. \tag{8}$$

The coefficients c_1 and c_2 were determined by minimising the root mean square (r.m.s.) difference in values of backscattering coefficient predicted by this formula and those observed. The best fit values were $c_1 = 0.000087$, $c_2 = 6.9$ and these gave an r.m.s error of 0.0047 in predicted backscattering coefficient. The backscattering efficiency can therefore be written as a function of the mineral fraction of particle mass as:

$$Q_{bb} = 0.000087 \exp(6.9.MSS/TSS). \tag{9}$$

This curve is shown in Fig. 4; it explains 62% of the variance in observed backscattering efficiency. Quadratic and power law forms for the variation of backscattering efficiency with *MSS/TSS* were also tried, with no improvement on this result.

We investigated whether the scatter of the points about the fitted curve depended on particle size. There was, however, no statistically significant relationship between the residual values of Q_{bb} and the particle size, expressed as either the Sauter diameter (D_A) or the median size by volume (D_{50}).

Organic material in the sea includes living phytoplankton cells and non-living detritus. It is likely that these two types of organic material will behave differently, optically, and that the *MSS/TSS* ratio we have used does not show this. Accordingly, we investigated the variation of backscattering efficiency with the ratio of chlorophyll to mineral suspended solids. At high chlorophyll:*MSS* ratios, the value of Q_{bb} was low, but at low and intermediate values of this ratio, there is a range of values of the backscattering efficiency. We conclude that, for this data set, chlorophyll is not a good predictor of Q_{bb}. This is a shame because chlorophyll is one of the products of remote sensing. It would be useful if the variation Q_{bb} could be estimated directly from remote sensing measurements.

3.4. Backscattering ratio b_b/b and MSS/TSS

Fig. 5 shows the backscattering ratio b_b/b plotted against the mineral content of the particles. The backscattering ratio shows a similar (but not identical) dependence on *MSS/TSS* to backscattering efficiency. For values of *MSS/TSS* < 0.7 the backscattering ratio has a value of about 0.005, it then rises to over 0.02 for the highest mineral proportions in our data set. Loisel, Meriaux, Berthon, and Poteau (2007) and Neukermans et al. (2012) also reported that the backscattering ratio in coastal seas increased with the fraction of mineral material. Boss et al. (2001) found a significant relationship between the backscattering ratio and the ratio of chlorophyll concentration to beam attenuation in the mid-Atlantic bight: as chlorophyll increased and particles became more organic b_b/b decreased from 0.035 to 0.005. Twardowski et al. (2001) predicted that the backscattering ratio will depend on the refractive index and the size distribution of the particles. We find no dependence of the backscattering ratio on particle size in our data set, however. Snyder et al. (2008) could find no relationship between the backscattering ratio and particle composition.

The change in b_b/b over the range of *MSS/TSS* values measured here is from about 0.005 to about 0.025, that is by a factor of 5. The change in backscattering efficiency over the same range of mineral content is greater: more like a factor of 10. As the proportion of mineral material increases, therefore, the particles scatter more light, but the backscattering increases more rapidly than total scattering, so that the backscattering ratio increases.

The mean value of b_b/b for this data set is 0.012 with a standard deviation of 0.006. This is comparable with two recent estimates of the backscattering ratio of 0.013 by Whitmire, Boss, Cowles, and Pegau (2007) and 0.0138 by Loisel et al. (2007).

4. Discussion

The long-term goal of this work is to improve our understanding of satellite images of seawater containing particulate material by gaining a greater insight to the way that marine particles react with light. In this paper we have shown that, as the mineral content of the particles increases, backscattering per unit particle area also increases. This conclusion agrees with the work of Flory et al. (2004) and Neukermans et al. (2012). It is encouraging that, though both these studies, and ours, used different instrumentation and sampled data in three different parts of the world, we have obtained similar results, both qualitatively and, to a large degree, quantitatively. The backscattering efficiency of

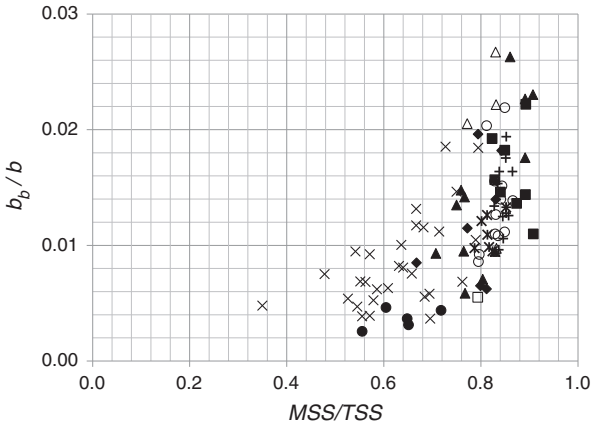

Fig. 5. Backscattering ratio b_b/b plotted against the MSS/TSS ratio. Note that there is a small difference in wavelength between the measurements of backscattering (665 nm) and scattering (670 nm).

suspended matter changes by an order of magnitude as the inorganic content of the aggregates changes from 35% to 90%.

The increase in backscattering efficiency with the mineral content of the particles is distinctly non-linear. The curve of backscattering efficiency against *MSS/TSS* ratio (Fig. 4) shows a gentle trend for mineral content below about 70% and a much steeper trend for mineral content above this. An exponential curve describes this behaviour reasonably well, although it could also be described by two straight lines, one for $MSS/TSS < 0.7$ and another for $MSS/TSS > 0.7$. Dividing the data into two parts, according to the mineral content of the particles, is consistent with the approach of McKee and Cunningham (2006, 2007) who found that the relationship between inherent optical properties and water constituents could be divided into two distinct groups (which they classified as sub-groups of the case-2 optical classification), based on the ratio of the chlorophyll concentration to mineral matter concentration.

The asymptotic value of Q_{bb} at low *MSS/TSS* ratios in Fig. 4 can be thought of as the backscattering efficiency of organic particles in the sea: whole and partial phytoplankton cells. A number of studies of the backscattering efficiency of marine phytoplankton have been made (Ahn et al., 1992; Whitmire, Pegau, Karp-Boss, Boss, & Cowles, 2010). Although the backscattering efficiency of many phytoplankton cells is less than 0.01, consistent with the curve drawn in Fig. 4, some species of phytoplankton have much higher values. Whitmire et al. (2010), for example, provides a table for phytoplankton with Q_{bb} lying in the range 0.006–0.267. The upper value of this range is much higher than the highest backscattering efficiency that we measured for mainly inorganic aggregates. Vaillancourt, Brown, Guillard, and Balch (2004) measured Q_{bb} at 440 nm for phytoplankton cells in the range 0.0023–0.081. The conclusion is that Q_{bb} at the lower end of the *MSS/TSS* scale is very variable and the curve fitted to our data and extrapolated into that range is just that: an extrapolation of our measurements.

A quantitative test of our 'understanding' of the processes that control the backscattering of light by aggregates is the proportion of the variance in b_b that can be explained by the processes that we propose. The cross-sectional area of particles in suspension clearly has an important role in controlling backscattering (Fig. 3). A linear regression of $b_b(665)$ against A explains 71% of the variance in b_b. There are, however, different trends in Fig. 3. If we now perform a linear regression of b_b against the *product* of A and Q_{bb} (calculated from Eq. 9) the proportion of explained variance increases from 0.71 to 0.89. Fig. 6 shows a plot of the backscattering coefficient against $Q_{bb}A$.

The fact that nearly nine-tenths of the variance in backscattering can be explained by changes in the cross-sectional area and mineral content of the particle is a striking result considering that it relies on three different types of measurement, each with its own difficulties and errors. Accurate gravimetric measurements of mass concentration are difficult to make, although it may help here that we are interested in the ratio of two masses, before and after baking the filters. The fact that triplicate measurements were made also reduces error in the *MSS/TSS* ratio. The LISST instruments that were used for measuring particle area are generally considered good for measuring spherical particles, but their ability to measure the area of particles of complex shape and structure is questionable. The LISST also has a limited range of size classes that it measures—with a lower limit of 2.5 μm. Finally, the backscattering measurements were made by combining data collected with a radiometer over a 10-metre water column and absorption measurements made in a sample collected near the surface. Despite the difficulties with these different measurements, they have combined in this case to give a coherent picture.

For some applications, it may be appropriate to convert remotely-sensed reflectance measurements into particle area. For example, some optical properties including the diffuse attenuation coefficient also scale with particle area (Bowers & Braithwaite, 2012). However, it is usually desirable to derive mass concentration from remote measurements of ocean colour over shelf seas and estuaries. This is because i) in situ measurements are usually in this form; ii) numerical models

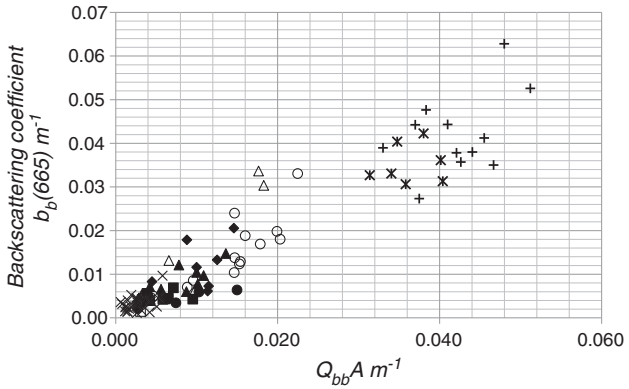

Fig. 6. Backscattering coefficient at 665 nm versus the product of backscattering efficiency (Eq. 9) and particle area.

predict mass concentration and iii) estimates of the flux of material are usually required in terms of the mass flux.

If we consider backscattering per unit mass of particles instead of per unit area, we can write the mass-specific backscattering coefficient b_b^* (by dividing both sides of Eq. 7 by mass concentration) as:

$$b_b^* = Q_{bb}A/TSS. \tag{10}$$

Fig. 7 shows a plot of b_b^* (calculated as $b_b(665)/TSS$) against the term $Q_{bb}A/TSS$, in which Q_{bb} was calculated from Eq. (9) and A and *TSS* were taken from the observations. A linear regression of b_b^* against $Q_{bb}A/TSS$, forced through the origin, gives the expression:

$$b_b^* = 1.01Q_{bb}A/TSS \tag{11}$$

($N = 97$, $R^2 = 0.61$, standard error of slope = 0.04).

The quantity $Q_{bb}A/TSS$ in Eq. (11) can be considered to consist of two parts. The first is the backscattering efficiency, Q_{bb}, which we have shown has a non-linear dependency on *MSS/TSS*. The second part, A/TSS, is the cross-sectional area of particles per unit mass. Because marine mineral matter is denser than marine organic material (typically by a factor of 2), aggregates with a higher mineral content will tend to have smaller area-to-mass ratio. Hill, Bowers, and Braithwaite (submitted for publication) shows that the area-to-mass ratio of aggregates decreases in a variable but approximately linear way with *MSS/TSS*. To some extent, therefore, the effect of particle mineral content on the two parts on the right hand side of Eq. (11) tends to cancel. Aggregates containing more mineral material have a higher refractive index and therefore are better at scattering light, but they also have a smaller cross-sectional area and so intercept fewer photons. The two effects do not cancel exactly,

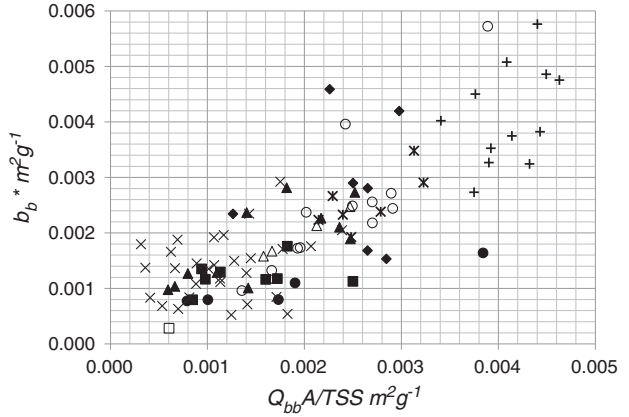

Fig. 7. Mass-specific backscattering coefficient, b_b^*, at 665 nm plotted against the backscattering efficiency (from Eq. 8) multiplied by the cross sectional area of particles per unit mass A/TSS.

however. The mass-specific backscattering coefficient has a weak, but statistically significant, dependence on *MSS/TSS* which, for our data set, can be expressed as:

$$b_b^* = -0.0016 + 0.00489 MSS/TSS \quad (12)$$

($N = 97$, $R^2 = 0.20$, standard error of intercept = 0.00077, standard error of slope = 0.0010). Particle size does not make a statistically significant contribution to this regression. Neukermans et al. (2012) found a similar weak dependence of b_b^* on particle composition. The conclusion for remote sensing of mass concentration of suspended aggregated matter, summarised by Fig. 7 and Eq. (9), is that the mass-specific backscattering coefficient depends on the cross-sectional area of the particles per unit mass moderated by an efficiency which depends on the *MSS/TSS* ratio. There is clearly much work to be done, however, in explaining the remaining variability in the mass-specific backscattering coefficient.

Acknowledgements

The authors are grateful to the Captain and crew of the RV Prince Madog and for technical staff at Bangor and Plymouth Universities who supported the fieldwork leading to this paper. We are grateful to Dr. Alex Nimmo-Smith and Dr. George Graham at Plymouth both for arranging the Plymouth Sound work and for many discussions about the difficulties of measuring tiny particles in sea water. This work was supported by a research grant from the UK Natural Environmental Research Council (NERC) and Defence Science and Technology Laboratory (dstl). The authors are grateful to two anonymous reviewers for helpful comments on the manuscript.

References

Agrawal, Y. C., & Pottsmith, H. C. (2000). Instruments for particle sizing and settling velocity observations in sediment transport. *Marine Geology*, *168*, 89–114.

Ahn, Y. -H., Bricaud, A., & Morel, A. (1992). Light backscattering efficiency and related properties of some phytoplankters. *Deep Sea Research*, *39*, 1835–1858.

Babin, M., Morel, A., Fournier-Sicre, V., Fell, F., & Stramski, D. (2003). Light scattering properties of marine particles in coastal and open ocean waters as related to the particle mass concentration. *Limnology and Oceanography*, *48*, 843–859.

Binding, C. E., Bowers, D.G., & Mitchelson-Jacob, E. G. (2005). Estimating suspended sediment concentrations from ocean colour in moderately turbid waters; the impact of variable particle scattering properties. *Remote Sensing of Environment*, *94*, 373–383.

Boss, E., & Pegau, W. S. (2001). Relationship of light scattering at an angle in the backward direction to the backscattering coefficient. *Applied Optics*, *40*, 5503–5507.

Boss, E., Pegau, W. S., Lee, M., Twardowski, M., Shybanov, E., Korotaev, G., et al. (2004). Particulate backscattering at LEO 15 and its use to study particle composition and distribution. *Journal of Geophysical Research*, *109*, C01014. http://dx.doi.org/10.1029/2002JC001514.

Boss, E., Slade, W., & Hill, P. (2009). Effect of particulate aggregation in aquatic environments on the beam attenuation and its utility as a proxy for particulate mass. *Optics Express*, *17*, 9408–9420.

Bowers, D.G., Boudjelas, S., & Harker, G. E. L. (1998). The distribution of fine suspended sediments in the surface waters of the Irish Sea and its relation to tidal stirring. *International Journal of Remote Sensing*, *19*, 2789–2805.

Bowers, D.G., & Braithwaite, K. M. (2012). Evidence that satellites sense the cross-sectional area of particles in shelf seas and estuaries better than their mass. *Geo-Marine Letters*, *32*, 165–171.

Bowers, D.G., Braithwaite, K. M., Nimmo-Smith, W. A.M., & Graham, G. W. (2011). The optical efficiency of flocs in shelf seas and estuaries. *Estuarine, Coastal and Shelf Science*, *91*, 341–350.

Cleveland, J. S., & Weidemann, A.D. (1993). Quantifying absorption by aquatic particles: A multiple scattering correction for glass-fibre filters. *Limnology and Oceanography*, *38*, 1321–1327.

Doxaran, D., Froidefond, J. -M., Castaing, P., & Babin, M. (2009). Dynamics of the turbidity maximum zone in a macrotidal estuary (the Gironde, France): Observations from field and MODIS satellite data. *Estuarine, Coastal and Shelf Science*, *81*, 321–332.

Eisma, D., Schumacher, T., Boekel, H., Hoerwaarden, J. V., Franken, H., Laan, M., et al. (1990). A camera and image-analysis system for in situ observations of flocs in natural waters. *Netherlands Journal of Sea Research*, *27*, 43–56.

Ellis, K. M., Binding, C. E., Bowers, D.G., Jones, S. E., & Simpson, J. H. (2008). A model of turbidity maximum maintenance in the Irish Sea. *Estuarine, Coastal and Shelf Science*, *76*, 765–774.

Flory, E. N., Hill, P.S., Milligan, T. G., & Grant, J. (2004). The relationship between floc area and backscatter during a spring phytoplankton bloom. *Deep Sea Research I*, *51*, 213–223.

Fugate, D. C., & Friedrichs, C. T. (2003). Controls on suspended aggregate size in partially mixed estuaries. *Estuarine, Coastal and Shelf Science*, *58*, 389–404.

Gallegos, C. L., Werdell, P. J., & McClain, C. R. (2011). Long term changes in light scattering in Chesapeake Bay inferred from Secchi depth, light attenuation and remote sensing measurements. *Journal of Geophysical Research*, *116*, C00H08. http://dx.doi.org/10.1029/2011JC007160.

Gordon, H. R., Brown, O. B., & Jacobs, M. M. (1975). Computed relationships between the inherent and apparent optical properties of a flat, homogenous ocean. *Applied Optics*, *14*, 417–427.

Graham, G. W., & Nimmo-Smith, W. A.M. (2010). The application of holography to the analysis of size and settling velocity of suspended cohesive sediments. *Limnology and Oceanography: Methods*, *8*, 1–15.

Graham, G. W., Davies, E. J., Nimmo-Smith, W. A. M., Bowers, D. G., & Braithwaite, K. M. (2012). Interpreting LISST 100X measurements of particles with complex shape using digital in-line holography. *Journal of Geophysical Research, (Oceans)*, *117*(C5). http://dx.doi.org/10.1029/2011 JC007613.

Gregory, J. (1989). Fundamentals of flocculation. *Critical Reviews in Environmental Control*, *19*, 185–230.

Hill, P.S., Bowers, D.G., & Braithwaite, K. M. (2014). The effect of suspended particle composition on particle area-to-mass ratios in coastal waters. *Ocean Optics* (submitted for publication August 2013).

Khelifa, A., & Hill, P.S. (2006). Models for effective density and settling velocity of flocs. *Journal of Hydraulic Research*, *44*, 390–401.

Kirk, J. T. O. (2011). *Light and photosynthesis in aquatic ecosystems* (3rd ed.). : Cambridge University Press.

Loisel, H., Meriaux, X., Berthon, J. -F., & Poteau, A. (2007). Investigation of the optical backscattering to scattering ratio of marine particles in the Eastern English Channel and Southern North Sea. *Limnology and Oceanography*, *52*, 739–752.

McKee, D., & Cunningham, A. (2006). Identification and characterisation of two optical water types in the Irish Sea from in situ inherent optical properties and seawater constituents. *Estuarine, Coastal and Shelf Science*, *68*, 305–316.

Milligan, T. G. (1996). In situ particle (floc) size measurements with the Benthos 373 plankton silhouette camera. *Journal of Sea Research*, *36*, 93–100.

Neil, C., Cuningham, D., McKee, D., & Polton, J. (2012). Remote sensing of seasonal stratification dynamics in the southern Irish Sea. *Remote Sensing of Environment*, *127*, 288–297.

Neil, C., Cunningham, A., & McKee, D. (2011). Relationships between suspended mineral concentrations and red-waveband reflectance in moderately turbid shelf seas. *Remote Sensing of Environment*, *115*, 3719–3730.

Neukermans, G., Loisel, H., Meriaux, X., Astoreca, R., & McKee, D. (2012). In situ variability of mass-specific beam attenuation and backscattering of marine particles with respect to particle size, density and composition. *Limnology and Oceanography*, *57*, 124–144.

Pope, R. M., & Fry, E. S. (1997). Absorption spectrum (380–700 nm) of pure water. II. Integrating cavity measurements. *Applied Optics*, *36*, 8710–8723.

Rivier, A., Gohin, F., Bryere, P., Petus, C., Guillou, N., & Chapalain, G. (2012). Observed vs. predicted variability in non-algal suspended particulate matter concentration in the English Channel in relation to tides and waves. *Geo-Marine Letters*, *32*, 139–151.

Snyder, W. A., Arnone, R. A., Davis, C. O., Goode, W., Gould, R. W., Ladner, S., et al. (2008). Optical scattering and backscattering by organic and inorganic particulates in US coastal waters. *Applied Optics*, *47*, 666–677.

Stramski, D., Boss, E., Bogucki, D., & Voss, K. J. (2004). The role of seawater constituents in light backscattering in the ocean. *Progress in Oceanography*, *61*, 27–50.

Twardowski, M. S., Boss, E., Macdonald, J. B., Pegau, W. S., Barnard, A. H., & Zaneveld, J. R. V. (2001). A model for estimating bulk refractive index from the optical backscattering ratio and the implications for understanding particle composition in case I and case II waters. *Journal of Geophysical Research*, *106*, 14129–14142.

Vaillancourt, R. D., Brown, C. W., Guillard, R. R. L., & Balch, W. (2004). Light backscattering properties of marine phytoplankton: Relationships to cell size, chemical composition and taxonomy. *Journal of Plankton Research*, *26*, 191–212.

Westberry, T. K., Dall'Olmo, G., Boss, E., Behrenfeld, M. J., & Moutin, T. (2010). Coherence of particle beam attenuation and backscattering coefficients in diverse open ocean environments. *Optics Express*, *18*, 15419–15425.

Whitmire, A. L., Boss, E., Cowles, T. J., & Pegau, W. S. (2007). Spectral variability of the particulate backscattering ratio. *Optics Express*, *15*, 7019–7031.

Whitmire, A. L., Pegau, W. S., Karp-Boss, L., Boss, E., & Cowles, T. J. (2010). Spectral backscattering properties of marine phytoplankton cultures. *Optics Express*, *18*, 15073–15093.